energies

MDPI

Article

Numerical and Thermodynamic Analysis of the Effect of Operating Temperature in Methane-Fueled SOFC

Berre Kumuk [1], Nisa Nur Atak [2], Battal Dogan [2], Salih Ozer [3], Pinar Demircioglu [4,5,*] and Ismail Bogrekci [5]

[1] Automotive Technologies Program Iskenderun Vocational School of Higher Education, Iskenderun Technical University, Hatay 31200, Türkiye; berre.kumuk@iste.edu.tr
[2] Energy Systems Engineering, Faculty of Technology, Gazi University, Ankara 06330, Türkiye; nisaatak28@gmail.com (N.N.A.); battaldogan@gazi.edu.tr (B.D.)
[3] Mechanical Engineering, Mus Alparslan University, Mus 49210, Türkiye; s.ozer@alparslan.edu.tr
[4] Institute of Materials Science, TUM School of Engineering and Design, Technical University of Munich, 85748 Garching, Germany
[5] Mechanical Engineering Department, Engineering Faculty, Aydin Adnan Menderes University, Aydin 09100, Türkiye; ibogrekci@adu.edu.tr
* Correspondence: pinar.demircioglu@tum.de

Abstract: This study examines the thermodynamic and numerical analyses of a methane-fed solid oxide fuel cell (SOFC) over a temperature range varying between 873 K and 1273 K. These analyses were conducted to investigate and compare the performance of the SOFC under various operating conditions in detail. As part of the thermodynamic analysis, important parameters such as cell voltage, power density, exergy destruction, entropy generation, thermal efficiency, and exergy efficiency were calculated. These calculations were used to conduct energy and exergy analyses of the cell. According to the findings, an increase in operating temperature led to a significant improvement in performance. At the initial conditions where the SOFC operated at a temperature of 1073 K and a current density of 9000 A/m^2, it was observed that when the temperature increased by 200 K while keeping the current density constant, the power density increased by a factor of 1.90 compared to the initial state, and the thermal efficiency increased by a factor of 1.45. Under a constant current density, the voltage and power density values were 1.0081 V, 1.0543 V, 2337.13 W/m^2, and 2554.72 W/m^2 at operating temperatures of 1073 K and 1273 K, respectively. Under a current density of 4500 A/m^2, the entropy generation in the cell was determined to be 29.48 kW/K at 973 K and 23.68 kW/K at 1173 K operating temperatures. The maximum exergy efficiency of the SOFC was calculated to be 41.67% at a working temperature of 1273 K and a current density of 1500 A/m^2. This study is anticipated to be highly significant, as it examines the impact of temperature variation on exergy analysis in SOFC, validating both numerical and theoretical results, thus providing a crucial roadmap for determining optimized operating conditions.

Keywords: solid oxide fuel cell (SOFC); numerical analysis; thermodynamic; energy; exergy; performance

Citation: Kumuk, B.; Atak, N.N.; Dogan, B.; Ozer, S.; Demircioglu, P.; Bogrekci, I. Numerical and Thermodynamic Analysis of the Effect of Operating Temperature in Methane-Fueled SOFC. *Energies* **2024**, *17*, 2603. https://doi.org/10.3390/en17112603

Academic Editor: Antonino S. Aricò

Received: 18 April 2024
Revised: 8 May 2024
Accepted: 24 May 2024
Published: 28 May 2024

1. Introduction

The continuous increase in energy demand today has led to a search for sustainable and environmentally friendly alternatives in the energy sector. Fuel cells have emerged as an innovative technological development designed to meet this need and provide a sustainable response to future energy demands [1]. Fuel cells represent significant diversity in the energy sector, with various types and application areas [2]. This technology, based on electrochemical reactions, aims to increase both environmental sustainability and energy efficiency. Solid oxide fuel cells (SOFCs), as seen in Figure 1, are a type of fuel cell composed of three basic components: anode, cathode, and electrolyte [3]. For the components of SOFC, state-of-the-art studies using mixed structures of various materials, such as perovskite and Ruddlesden–Popper, are available [4,5]. SOFCs stand out among other fuel cells

due to their high-performance operation at elevated temperatures. SOFCs operating at high temperatures attract attention due to their ability to utilize a wide range of fuels [6]. Thanks to these features, SOFCs provide fuel flexibility in energy production, effectively utilizing various fuel sources such as hydrogen, biogas, and methane. Experimental and numerical studies on the use of hydrocarbon-based fuels in SOFCs are documented in the literature [7–13]. Rath et al. conducted a performance analysis of an anode-supported SOFC under various operating conditions. In the study, the anode electrode of the SOFC was fueled with hydrocarbon fuel. It was observed that increasing the temperature had a positive effect on performance, while increasing the current density had a negative effect on performance [14]. Randolph et al. experimentally examined the performance of an SOFC operating with various hydrocarbon fuels at different operating pressures and temperatures. According to the obtained data, the best fuel feeding was observed with methane fuel [15].

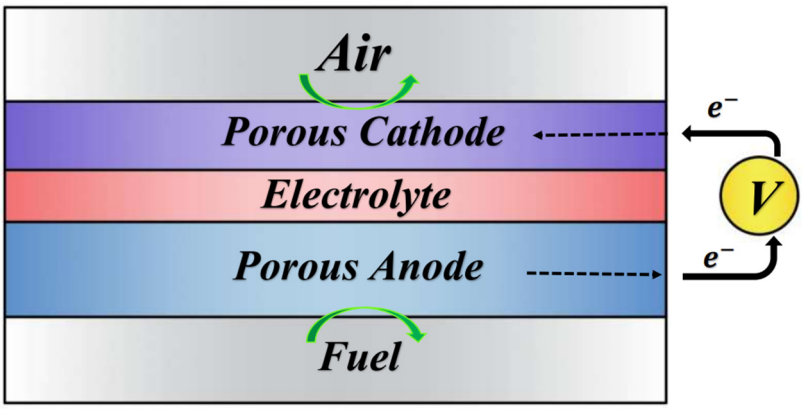

Figure 1. Direct reformed anode-supported SOFC configurations.

In SOFCs, hydrocarbon-based fuels are typically used in the cell through direct or indirect internal reforming methods. These methods involve the generation of fundamental reaction products such as hydrogen and carbon monoxide within the fuel cell, participating in the energy conversion processes [16]. Methane reforming is a method used in energy production systems for high-temperature operating SOFCs. This process represents an indirect processing step that enables the efficient utilization of hydrogen-containing hydrocarbon fuels, such as methane, by solid oxide fuel cells. Researchers have conducted numerical analyses by modeling SOFC systems where methane undergoes an indirect reforming process, including pre-processing [17–21].

The utilization of hydrocarbon-containing fuels like methane directly in SOFCs offers simplification potential by eliminating the need for a separate system to convert the fuel into hydrogen [22,23]. Additionally, this method reduces costs and optimizes energy conversion processes. In the literature, numerous experimental studies are focusing on directly feeding methane to the anode electrode of the SOFC [24–29]. Lin et al. conducted an energy analysis of a directly methane-fueled, Ni-YSZ (nickel-yttria-stabilized zirconia) electrode-supported SOFC at different operating temperatures. The use of methane resulted in a decrease in fuel cell voltage compared to hydrogen, leading to a lower power density. At a working temperature of 700 °C, while the voltage obtained using hydrogen as fuel was 0.55 V, this voltage dropped to 0.3 V when methane fuel was used. Additionally, both the cell potential and power density increased with increasing operating temperature [16]. Fu et al. calculated performance parameters, such as the cell potential and power density, of a directly methane-fueled SOFC in their study. According to the results obtained, high operating temperatures positively influenced cell performance, providing maximum values. These maximum voltage and power density values were 1.02 V and 0.45 W/cm^2, respectively [18].

Some studies in the literature have examined the energy and exergy analysis of SOFC under direct methane reforming [30,31]. These studies hold significant importance in

understanding and optimizing the performance of SOFC during the methane-reforming process. Heidarshenas et al. conducted a performance analysis of an SOFC system with methane reforming. The variation in operating pressure and temperature significantly affected the performance. The maximum SOFC power was calculated to be 15,000 W at 1200 °C temperature and 5600 W at 2000 kPa pressure, respectively [32]. Singh and Bhogilla conducted an energy and exergy analysis of a methane-fueled SOFC system at different temperatures and various current densities. Increasing the temperature up to the optimum point increased the energy and exergy efficiency of the SOFC. The exergy efficiency was calculated to be 38% at the optimum temperature of 900 K [33].

A literature review revealed that the performance of direct methane-fueled solid oxide fuel cells has been examined under various parameters using different computational fluid dynamics programs [34–36]. Xie et al. numerically examined solid oxide fuel cells operated with direct methane at 600 °C, 650 °C, and 700 °C. The analysis results indicated that the anode reaction processes in SOFCs operated with direct methane were slower than the cathode oxygen reduction process. The results also explained that water (H_2O) could enhance cell performance by intensifying methane-reforming reactions. Increasing the inlet methane flow rate was observed to improve cell performance and enhance the methane-reforming process by producing more steam [6]. Iliev et al. investigated the performance of SOFC by simulating it with hydrogen, methane, and syngas using COMSOL Multiphysics. In their study, it was observed that the SOFC produced 1340 W/m^2 power with a current density of 0.25 A/cm^2 when operated with hydrogen, and 1200 W/m^2 at the same current density when operated with methane. When syngas was used, the power density reached 1340 W/m^2 at a current density of 0.3 A/cm^2 [37].

This study aims to investigate the effect of temperature on the performance of SOFC via numerical and thermodynamic analysis. When the studies in the literature are examined, SOFC efficiency increases at high temperatures. However, this increase is not continuous. In this study, thermal efficiency and exergy efficiency were calculated by thermodynamic analysis to determine the optimum operating temperatures. The optimum operating temperatures were determined by examining the effect of the decrease in power density on thermal efficiency and exergy efficiency when the temperature was too high or too low. As an addition to the literature, it is predicted that this study will be important in terms of examining the effect of temperature change on exergy destruction and exergy efficiency in SOFC. Table 1 shows the comparison of recent findings with the literature.

Table 1. Comparison of recent findings with the literature.

Reference	Active Cell Area [m^2]	Operating Temperature [K]	Current Density [A/m^2]	Cell Potential [V]	Power Density (W/m^2)
The present study	0.01 m^2	873–1273 K	0–12,000 A/m^2	0–1.22 V	0–13,000 W/m^2
Zhao and Virkar [38]	0.02 m^2	873–1073 K	0–30,000 A/m^2	0.1–1.12 V	0–12,000 W/m^2
Altindal et al. [3]	-	873–1273 K	0–0.7 A/m^2	0.35–1.13 V	0.02–0.24 W/m^2
Wang et al. [39]	-	973–1073 K	0–5000 A/m^2	0.68–1.25 V	0–0.45 W/cm^2

2. Materials and Methods

Solid oxide fuel cells generally operate between temperatures of 800 K and 1200 K. In this study, voltage and current densities were calculated at 1073 K, 1173 K, and 1273 K in numerical analysis, and these data were compared with the voltage and current densities found by theoretical calculations. In the exergy analysis, calculations were made at temperatures of 1073 K, 1173 K, and 1273 K. After the literature comparison, calculations of 873 K and 973 K temperatures were added.

2.1. Numerical Analysis

The geometry of the anode-supported SOFC used in the analysis is depicted in Figure 2. The SOFC consists primarily of thin, porous cathode and anode layers, an electrolyte, and flow channels for both the anode and cathode. The porous anode, electrolyte, and cathode layers can be characterized with homogeneous and effective parameters (such as effective porosity, permeability, and thermal conductivity). As observed, methane and oxygen flows are counter-current. Additionally, it is assumed that the phase in contact with the flow is thermally stable. The electrolyte layer is thin enough to facilitate enhanced ion transfer, while the anode layer is thick enough to support the cell.

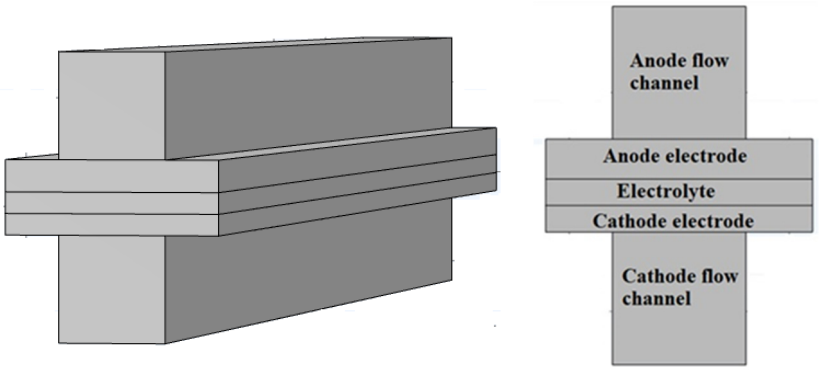

Figure 2. COMSOL Multiphysics model view of the SOFC: (**a**) 3D geometry of the model. (**b**) Cross-sectional view of the model.

The geometric input parameters used in the SOFC model are as shown in Table 2.

Table 2. SOFC system design parameters [40–44].

Items	Unit	Value
Active cell area, A	[m^2]	0.01
Gas flow channel width	[m]	0.5×10^{-3}
Rib width	[m]	0.5×10^{-3}
Anode electrode thickness, t_a	[m]	1.5×10^{-4}
Cathode electrode thickness, t_c	[m]	10^{-4}
Electrolyte thickness, t_e	[m]	10^{-4}
Gas flow channel height	[m]	0.5×10^{-3}
Flow channel length	[m]	0.01 m
Average pore radius, D_p	[m]	2×10^{-6}
Average grain size, D_s	[m]	1.5×10^{-6}
Porosity, n	-	0.4
Permeability	[m^2]	10^{-10} m^2
Anode's tortuosity, ξ	-	5.4
Average grain contact length, X	-	0.7
Symmetrical factor, α	-	0.5

Figure 3 shows the workflow diagram of the SOFC model in COMSOL Multiphysics.

As shown in Figure 3, the workflow of a solid oxide fuel cell (SOFC) model in COMSOL Multiphysics typically includes the following steps: The first step is to create the geometry of the fuel cell. This involves placing electrodes, electrolyte layers, and other components. The second step involves determining the properties of the materials used. Properties such as conductivity, thermal conductivity, diffusion coefficient of electrodes, electrolyte, and other components are defined at this stage. Next, equations representing different physical processes such as electrochemical reactions, heat transfer, mass transfer, and electrical behavior are defined. These equations describe various phenomena occurring

within the fuel cell. In addition to chemical reactions occurring in the electrodes, multiple physical processes such as heat and mass transfer are also modeled. Boundary conditions determine how interactions outside the system are modeled. For example, conditions such as potential differences in the electrodes, boundary transitions of fluids, and heat losses are determined here. The geometry is divided into analyzable parts using the finite element method. This step involves creating the computational mesh used in finite element analysis. As the model approaches completion, it is simulated under the defined equations and boundary conditions. COMSOL performs this simulation depending on computational power and the selected solver. In the final step, simulation results are visualized and analyzed. This includes examining various parameters such as electrode performance, temperature distribution, and fluid behavior.

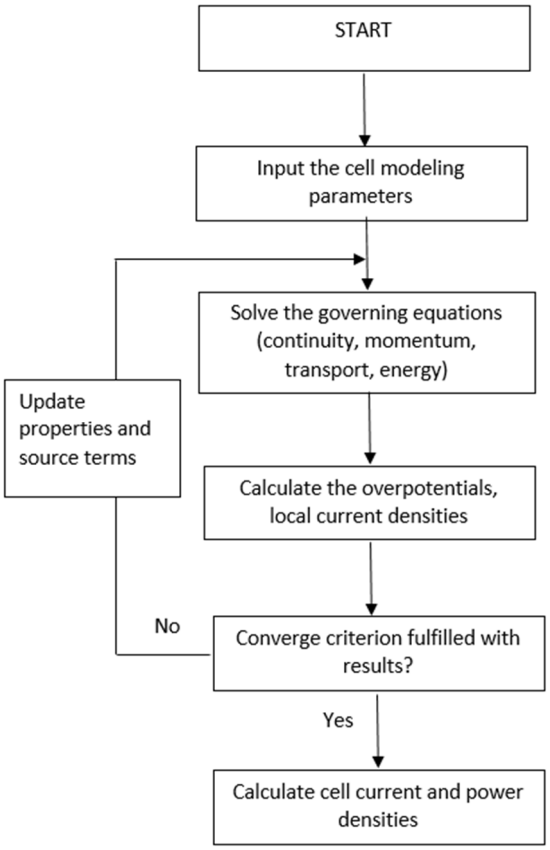

Figure 3. Workflow diagram of the numerical model.

2.2. Thermodynamic Analysis

The thermodynamic analysis of an SOFC is an important methodology that determines the energy balance and performance of the cell. The chemical reactions and energy transfer occurring within the cell are examined according to thermodynamic principles. While the anode electrode contains hydrogen molecules, the cathode electrode contains oxygen molecules, which act as the oxidizer.

$$Anode: \ 2H_2 + 2O_2 \rightarrow 2H_2O + 4e^- \quad (1)$$

$$Cathode: \ O_2 + 4e^- \rightarrow 2O^{-2} \quad (2)$$

$$Total\ cell\ reaction: \ 2H_2 + O_2 \rightarrow 2H_2O \quad (3)$$

During electrochemical reactions in an SOFC, activation (η_{act}), ohmic (η_{ohmic}), and concentration (η_{conc}) losses occur. The equilibrium potential (E) is a point where the rates of electrochemical reactions are equal, and the cell operates at a constant voltage.

The cell voltage (V) is obtained by subtracting the losses occurring in the cell from the equilibrium potential.

$$V = E - \eta_{act} - \eta_{conc} - \eta_{ohmic} \quad (4)$$

In the calculation of equilibrium potential, the pressures of hydrogen, oxygen, and water $\left(P_{H_2}, P_{O_2}\ and\ P_{H_2O}\right)$ are influential. Equation (6) provides the temperature-dependent expression for the reversible potential (E_0) [41]:

$$E = E_0 + \frac{RT}{2F}\ln\left(\frac{P_{H_2}{P_{O_2}}^{1/2}}{P_{H_2O}}\right) \quad (5)$$

$$E_0 = 1.253 - 2.451 \times 10^{-4}\ T \quad (6)$$

Table 3 provides equations defining the losses occurring within the cell for the purpose of calculating the SOFC cell potential (V). These equations describe various loss mechanisms such as activation, ohmic, and concentration losses. Activation loss represents the amount of energy required for gases to react on the electrode surfaces, while ohmic losses represent the resistance loss between the electrodes. Concentration loss includes losses arising from the concentration contents of gases on the electrode surfaces. These equations serve as fundamental tools for calculating the cell potential and play a significant role in understanding the performance of the SOFC. Additionally, Table 3 presents the input conditions that will form the basis of the calculations. Also, Table 4 shows that the Inlet operating conditions.

Table 3. Equations for the calculation of cell losses in SOFC [40–43,45,46].

Nernst Equation	
Activation overpotential equation	$\eta_{act,i} = \frac{RT}{F} sinh^{-1}\left(\frac{J}{2J_{0,i}}\right)$; i = a, c $J_{0,a} = k_a \frac{72\times\left[D_p-\left(D_p+D_s\right)n\right]n}{{D_s}^2{D_p}^2\left(1-\sqrt{1-X^2}\right)} \times \left(\frac{P_{H_2}}{P_{ref}}\right)\left(\frac{P_{H_2O}}{P_{ref}}\right) \exp\left(-\frac{E_{act,a}}{RT}\right)$ $J_{0,c} = k_c \frac{72\times\left[D_p-\left(D_p+D_s\right)n\right]n}{{D_s}^2{D_p}^2\left(1-\sqrt{1-\alpha^2}\right)} \times \left(\frac{P_{O_2}}{P_{ref}}\right)^{0.25} \exp\left(-\frac{E_{act,c}}{RT}\right)$
Concentration overpotential equation	$\eta_{conc,a} = \frac{RT}{2F}\ln\left[\frac{1+\frac{RTt_aJ}{2FD_a^{eff}P^0_{H_2O}}}{1-\frac{RTt_aJ}{2FD_a^{eff}P^0_{H_2}}}\right]$ $\eta_{conc,c} = \frac{RT}{2F}\ln\left[\frac{1}{1-J/J_{L,O_2}}\right]$ $\frac{1}{D_a^{eff}} = \frac{\xi}{n}\left(\frac{1}{D_{H_2-H_2O}} + \frac{1}{D_{H_2,k}}\right)$ $\frac{1}{D_c^{eff}} = \frac{\xi}{n}\left(\frac{1}{D_{O_2-N_2}} + \frac{1}{D_{O_2,k}}\right)$
Ohmic overpotential equation	$\eta_{ohmic} = 2.99 \times 10^{-11} J\ t_e\ exp\left(\frac{10{,}300}{T}\right)$

Table 4. Inlet operating conditions [40].

Items	**Unit**	**Value**
Faraday constant, ***F***	[C/mol]	96,485
Universal gas constant, ***R***	[J/mol K]	8.3145
Temperature of operation, ***T***	[K]	1073–1273
The pressure of operation, ***P***	[bar]	1
Anode activation energy, $E_{act,a}$	[J/mol]	1.344×10^{10}
Cathode activation energy, $E_{act,c}$	[J/mol]	2.051×10^{9}

The control volume of the SOFC establishes a mass balance by tracking the movement of gases within the system. In this volume, hydrogen and oxygen inlets occur, while water and oxygen outlets are observed. Maintaining balance is critical for ensuring the correct flow of gases within the cell and the effective occurrence of reactions. This process plays a

fundamental role in the operation of the SOFC and has a significant impact on the efficiency of the system. The following equations provide the mass balance in the control volume [47]:

$$\dot{n}_{out,H_2} = \dot{n}_{in,H_2} - \dot{z} \tag{7}$$

$$\dot{n}_{out,H_2O} = \dot{n}_{in,H_2O} + \dot{z} \tag{8}$$

$$\dot{n}_{out,O_2} = \dot{n}_{in,O_2} - \frac{\dot{z}}{2} \tag{9}$$

$$\dot{n}_{out,N_2} = \dot{n}_{in,N_2} \tag{10}$$

The molar flow rate ($\dot{n}$) and fuel utilization factor (U_f) are multiplied to obtain the number of moles of hydrogen $(\dot{z})$ [47]:

$$\dot{z} = U_f \dot{n}_{in,H_2} \tag{11}$$

The molar flow rate of oxygen ($\dot{n}_{in,O_2}$) is calculated based on the fuel utilization factor and the number of moles, as stated in reference [47]:

$$\dot{n}_{in,O_2} = \frac{\dot{z}}{2U_f} \tag{12}$$

Thermal efficiency is an important parameter that indicates how much of the energy from the fuel is converted into electrical energy. The thermal efficiency of the SOFC is determined by comparing the power output of the cell ($\dot{W}_{FC}$), to the fuel energy input (F_{in}).

$$\eta_{thermal} = \frac{\dot{W}_{FC}}{F_{in}} \tag{13}$$

The energy balance in a fuel cell is based on the principle that the total energy of the fuel and air flow entering the cell in terms of chemical energy is equal to the total energy of the electricity and heat energy leaving the cell [48,49].

$$\dot{Q} - \dot{W} = \sum_i \dot{n}_i \overline{h}_i - \sum_e n_e \overline{h}_e \tag{14}$$

Exergy analysis in an SOFC is a vital tool for evaluating the efficiency of energy conversion processes. The concept of exergy represents the potential of the system's internal energy to be converted into usable work externally. It also assesses the system's efficiency and energy quality, providing information about its capacity to perform work. As shown in the following equations, the exergy of the system is obtained by summing the chemical and physical exergies [50]. The data provided in Table 5 are used for these calculations.

$$\dot{Ex} = \dot{Ex}^{ph} + \dot{Ex}^{ch} \tag{15}$$

$$\dot{Ex}^{ph} = \sum_i \dot{n}_i \left(\overline{h}_i - \overline{h}_0\right) - T_0 \left(\overline{s}_i - \overline{s}_0\right) \tag{16}$$

$$\dot{Ex}^{ch} = \dot{n}\left(\sum_i y_i \overline{ex}_i^{ch,0} + \overline{R} T_0 \sum_i y_i \ln y_i\right) \tag{17}$$

Exergy destruction in an SOFC represents the losses in the energy conversion process of the system. Exergy destruction is a parameter that decreases the efficiency of the system and identifies unwanted energy losses. Minimizing exergy destruction plays a significant role in increasing cell efficiency.

$$\Delta \dot{Ex}_{dest} = \left(\dot{Ex}_{O_2} + \dot{Ex}_{H_2}\right) - \left(P + \dot{Ex}_{out,\,O_2} + \dot{Ex}_{out,\,H_2O}\right) \tag{18}$$

$$\Delta S = \frac{\Delta \dot{Ex}_{dest}}{T_0} \tag{19}$$

Exergy efficiency is typically calculated by comparing the work obtained in the cell to the total energy contained in the fuel. A low exergy efficiency indicates that the system operates inefficiently and potentially wastes valuable energy. On the other hand, a high exergy efficiency represents that the system can use and convert energy more efficiently [46].

$$\eta_{exergy} = \frac{\dot{W}_{FC}}{E\dot{x}_{in}} \times 100 \quad (20)$$

Table 5. Properties in the standard-state condition [51].

Parameters	Value
$\mathbf{C_{p,air}}$	1.005 kJ/kg K
$\mathbf{C_{p,H_2}}$	14.3 kJ/kg K
$\mathbf{C_{p,O_2}}$	0.918 kJ/kg K
$\boldsymbol{\lambda_{O_2}}$	3 kJ/kg K
$\mathbf{s_{0,O_2}}$	129.17 kJ/kmol K
$\mathbf{s_{0,H_2O}}$	0.3674 kJ/kmol K
$\mathbf{h_{0,O_2}}$	−21.120 kJ/kg K
k	1.4

3. Results and Discussion

This study focuses on the thermodynamic and numerical analyses of a direct methane-fueled solid oxide fuel cell (SOFC) over different temperature ranges (873 K–1273 K). The primary objective of these analyses is to thoroughly examine the performance of the SOFC under various operating conditions and provide a comparative perspective. In this way, the effects of temperature variations on the efficiency and energy conversion capacity of the cell have been evaluated more comprehensively.

3.1. Numerical Results

The developed mathematical models were numerically investigated using the COMSOL Multiphysics (version 6.2 program). The software utilized includes a solid oxide fuel cell module for numerical modeling. Within this module, an anode-supported solid oxide fuel cell was developed under different operating conditions with direct methane utilization and analyzed at various temperature values (1073 K, 1173 K, and 1273 K).

In SOFC modeling, the selection of key materials plays a pivotal role in determining cell performance. Materials such as electrolytes, electrodes, and interconnects directly impact the efficiency, stability, and overall functionality of the cell. For instance, the electrolyte material must exhibit high ionic conductivity at operating temperatures to facilitate efficient ion transport. Similarly, electrode materials need to possess high catalytic activity for the respective electrochemical reactions involved while also maintaining structural stability under harsh operating conditions. Furthermore, the choice of interconnect material is critical for ensuring good electrical conductivity and mechanical integrity, as it connects individual cells within the stack. Therefore, a comprehensive understanding of material properties and their interactions is essential for accurate modeling and optimization of SOFC performance. Thus, in this study, the cell materials are yttria-stabilized zirconia (YSZ: 8 mol%Y_2O_3-ZrO_2) for the electrolyte, nickel oxide (NiO)/YSZ (wt.%: 60/40) for the anode, and $La_{0.60}Sr_{0.40}FeO_3$-d (LSF) for the cathode.

3.1.1. The Methane (CH4) Mole Distribution at Different Temperatures

This study examines the effect of direct methane utilization on the performance of SOFCs under different temperature conditions. Figure 4 illustrates contour plots of methane mole distribution at different temperatures. In solid oxide fuel cells with direct methane utilization, the distribution of methane molecules in the anode layer is affected by temperature changes. As the temperature increases, the oxidation rate of methane increases, leading to accelerated oxidation reactions of methane in the anode layer and

the formation of by-products. Thus, at higher temperatures, methane molecules oxidize more rapidly on the anode surface, potentially speeding up the process of conversion to by-products such as carbon dioxide (CO_2) and water (H_2O). Another reason for this phenomenon is the increase in diffusion and reaction rates. Typically, as the temperature increases, the diffusion rates of gas molecules also increase, allowing for more effective reactions within the cell. The oxidation of methane in the anode layer requires the gas to reach the electrode surface and participate in reactions. Higher temperatures can accelerate such diffusion processes. Additionally, thermokinetic factors influence the methane mole distribution. Temperature affects thermokinetic factors that influence reaction kinetics. The activation energy of reactions may decrease with temperature, leading to increased reaction rates. Ultimately, when these factors come together, the oxidation reactions of methane in the anode layer accelerate at high temperatures, resulting in increased conversion of methane to carbon dioxide and water. This phenomenon may contribute to the more efficient operation of SOFCs and higher energy conversion efficiency. Consequently, the enhanced oxidation and diffusion processes at elevated temperatures contribute to a more uniform distribution of methane across the anode layer, facilitating a more consistent and efficient reaction environment.

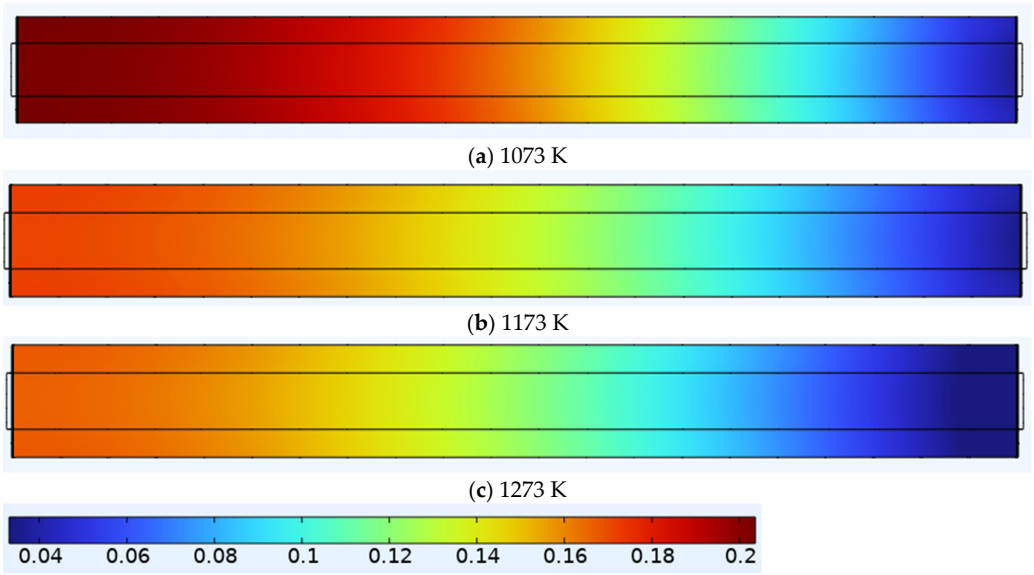

Figure 4. Methane mole distribution at (**a**) 1073 K, (**b**) 1173 K, and (**c**) 1273 K temperatures (V = 0.8 V).

3.1.2. Electrolyte Current Density at Different Temperatures

This study investigates the effect of direct methane utilization on the current density of SOFCs at different temperature conditions, as depicted in Figure 5 with contour plots. Changes in electrolyte current density in direct methane-fueled SOFCs with increasing temperature are influenced by several factors. Firstly, electrochemical reaction rates play a significant role. Generally, at high temperatures, electrochemical reaction rates increase. In SOFCs, oxidation and reduction reactions occur at the electrodes. An increase in temperature can enhance these reactions, thereby increasing electrochemical activity and, consequently, electrolyte current density. Another reason is the increase in diffusion and conductivity. With increasing temperature, faster diffusion of gas molecules and ions between electrodes becomes possible. Additionally, enhanced ion conduction and electron conductivity in the electrodes improve interactions between electrodes, contributing to the increase in electrolyte current density. Another significant factor is thermokinetic factors. An increase in temperature can reduce the activation energy of electrochemical reactions, allowing reactions to occur at lower energy levels and potentially leading to higher current densities. Furthermore, the reaction rates of methane fuel and oxygen used in SOFCs are temperature-dependent. The increased rate of these reactions can enhance participation in

electrochemical reactions, thereby increasing electrolyte current density. When these factors are combined, it is observed that the electrolyte current density of SOFCs increases at high temperatures. Moreover, the overall performance and efficiency of SOFCs improve at higher temperatures due to the combined effects of increased reaction rates, faster diffusion, and reduced activation energy.

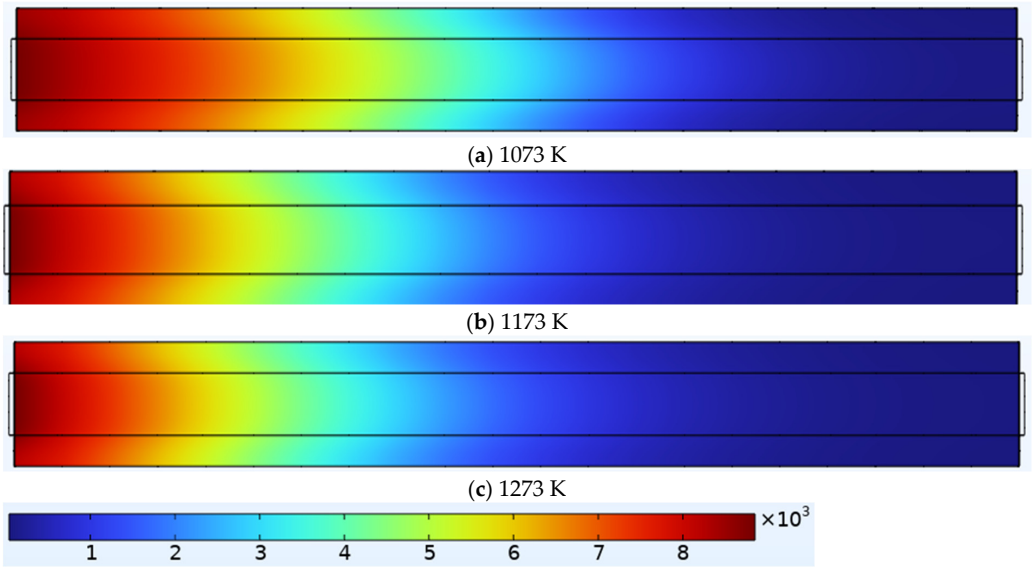

Figure 5. Electrolyte current density at (**a**) 1073 K, (**b**) 1173 K, and (**c**) 1273 K temperatures (V = 0.8 V).

3.1.3. Validation of Numerical Results

This study demonstrates a high degree of consistency between the numerical and theoretical analyses, as observed in Figure 6, indicating a robust validation process. The validation presented at a working temperature of 1273 K is consistent with similar approaches at other temperatures. The results of numerical modeling show consistency with theoretical analyses, confirming that the numerical modeling accurately captures the thermodynamic behavior of the system. This coherent validation enhances the reliability of the study, indicating that the results obtained are based on a solid foundation.

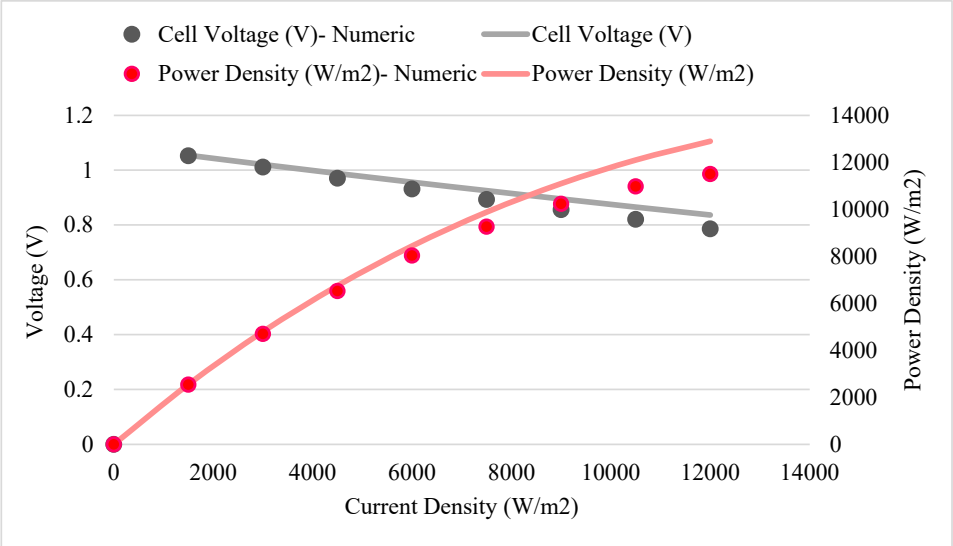

Figure 6. Validation between numerical and thermodynamic results obtained at 1273 K temperature.

The clear consistency between theoretical analysis and numerical modeling emphasized in this study provides a strong basis for understanding and optimizing the thermodynamic behavior of our system.

3.2. Thermodynamics Results

The thermodynamic analyses examine a series of parameters critical for assessing SOFC performance. These parameters include flow rate, cell voltage, power density, entropy production, exergy destruction, and thermal and exergy efficiency. However, the most crucial aspect is determining the irreversibilities and entropy generation encountered by the SOFC under different operating conditions. Irreversibilities and entropy generation are factors affecting the efficiency of the SOFC and, thus, directly impacting its performance. High entropy generation is associated with low energy efficiency. Therefore, minimizing entropy generation and irreversibilities is crucial for enhancing the performance of the SOFC.

In Figure 7, the cell voltage of the SOFC at different temperatures is provided, while Figure 8 illustrates power density. The cell voltage of an SOFC is the electrical potential resulting from electrochemical reactions occurring within the cell, converting chemical energy supplied by the fuel and oxidant into electrical energy. Power density, on the other hand, is a parameter measuring the electrical performance of the cell. It is calculated by multiplying cell voltage and current density. Thus, power density is directly related to the relationship between cell voltage and current density. Therefore, to achieve optimal power density, maximizing cell voltage and maintaining current density at an appropriate level are necessary. At a current density of 1500 A/m^2 and 1273 K temperature conditions, the cell voltage of the SOFC is 1.0543 V. Liu and Barnett [52] experimentally investigated the performance of a methane-fueled, anode-supported SOFC. According to the obtained data, increasing the operating temperature increased both cell voltage and power density. However, an increase in current density reduced cell performance, which is contrary to this positive effect. This situation demonstrates the complex interactions affecting the electrical performance of the SOFC. The maximum power density in the cell was observed to be 0.81 W/cm^2 at a temperature of 800 °C and a 1.25 A/cm^2 current density.

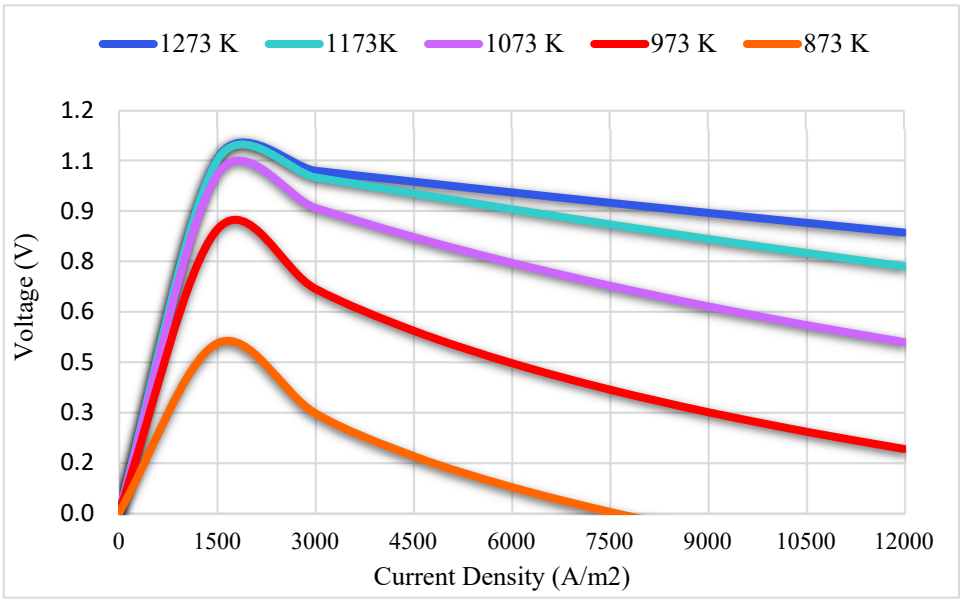

Figure 7. Cell voltages at different operating temperatures in SOFC.

As the operating temperature increased, it was observed that the cell voltage increased, leading to a more efficient energy conversion. This resulted in an increase in power density. By keeping the current density constant, increasing the operating temperature from

1073 K to 1173 K increased the power density by 41.27% compared to the initial condition. At an operating temperature of 1073 K and a current density of 6000 A/m^2, the values of cell voltage and power density were 0.7462 V and 5567.431 W/m^2, respectively. Tu et al. [53] experimentally and thermodynamically examined the performance of a methane-fueled SOFC in various operating temperature ranges (773 K–1073 K). It was observed that increasing the operating temperature in the SOFC resulted in an improvement in cell performance. At 923 K and 1073 K operating temperatures and the same current density, the cell voltages were 0.37 V and 0.78 V, respectively.

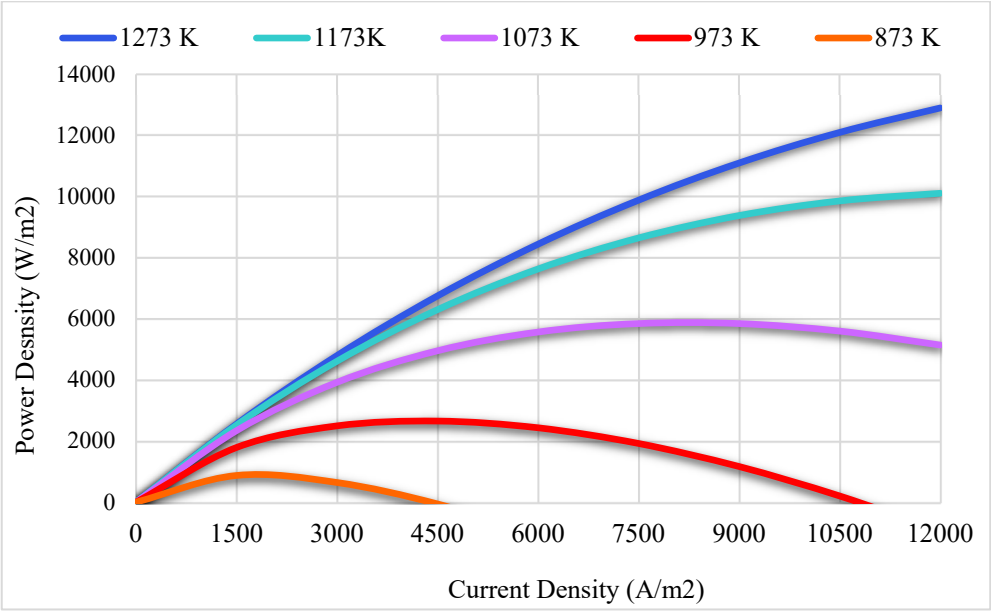

Figure 8. Power densities at different current densities in SOFC.

Exergy destruction represents the portion of exergy in a system that cannot be converted into useful work within or outside the system. In SOFCs, exergy destruction typically occurs due to losses within the cell, resistances, and reaction inefficiencies. These losses decrease the efficiency and performance of the system, hindering the full utilization of the exergy potential. In Figure 9, the exergy destruction in SOFC at different current densities is provided. The increase in operating temperature led to a decrease in exergy destruction in the SOFC. By keeping the current density constant, increasing the operating temperature from 973 K to 1273 K reduced the exergy destruction by 37.953% compared to the initial condition. At a current density of 6000 A/m^2, the exergy destruction of the SOFC at 1173 K and 873 K operating temperatures was 14,440.78 kW and 9693.06 kW, respectively. The maximum exergy destruction was calculated to be 31,691.37 kW at 873 K and 12,000 A/m^2 current density.

Entropy is a thermodynamic concept that represents the degree of disorder or randomness in a system. In SOFCs, entropy production arises from factors such as heat transfer in the cell, chemical reactions, and cell losses. Processes like electrochemical reactions, ion and electron transfer, and molecular motion and disorder contribute to entropy production. This entropy production is a consequence of the thermal and chemical characteristics of the system and is a significant factor affecting the energy conversion efficiency of the system. Minimizing entropy production in SOFCs is crucial because minimal entropy allows the cell to operate at maximum performance. As shown in Figure 10, a decrease in operating temperature leads to an increase in entropy production. At 1173 K and 1073 K operating temperatures and 9000 A/m^2 current density, entropy production was 51.470 kW/K and 57.138 kW/K, respectively. With a constant current density condition, increasing the operating temperature by 45.81% reduced the entropy production by 32.59 kW/K compared to the initial condition.

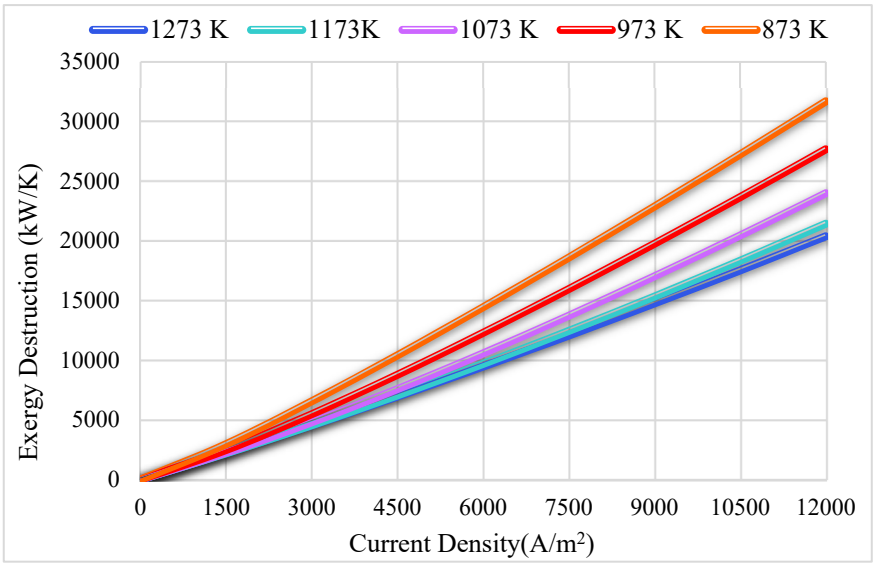

Figure 9. Exergy destruction at different current densities in SOFC.

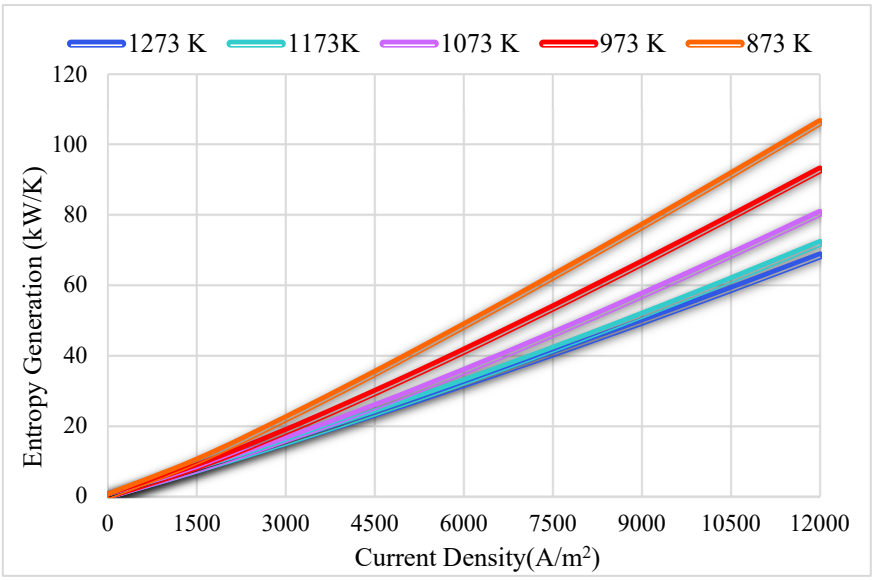

Figure 10. Entropy production at different current densities in SOFC.

This increase in entropy production at lower operating temperatures can result in reduced efficiency and performance of the SOFC. Consequently, careful control and optimization of operating temperatures and other system parameters are essential to maintaining low entropy production levels and maximizing energy conversion efficiency. By managing entropy production effectively, the overall operational lifespan of the SOFC can also be extended.

In Figure 11, the thermal efficiency of SOFC at different temperatures is provided, while Figure 12 shows the exergy efficiency. Thermal efficiency in a fuel cell is defined as the ratio of the energy obtained from the fuel to the electrical energy generated in the cell, while exergy efficiency is expressed as the ratio of the energy obtained from the fuel to the maximum theoretical energy. Thermal efficiency indicates how effective the cell is in electricity generation, while exergy efficiency denotes the efficiency of energy conversion in the cell. These parameters play a crucial role in evaluating the performance of SOFCs. As the operating temperature of the SOFC increased, the cell exhibited better performance, leading to an increase in both energy and exergy efficiency. At 3000 A/m^2 current density

and a temperature of 973 K, the thermal and exergy efficiencies were 30.29% and 26.78%, respectively. The maximum thermal and exergy efficiency was calculated to be 47.76% at a 1273 K operating temperature and 1500 A/m² current density. It was observed that high temperatures, up to a certain point, allowed the cell to perform better, resulting in higher efficiency. Saebea et al. [24] conducted a study analyzing the performance of a direct methane-fueled SOFC at various operating temperatures (600–750 °C), comparing numerical and experimental results. An increase in the operating temperature resulted in a significant improvement in the cell performance. Increasing the operating temperature from 650 °C to 750 °C under constant conditions increased the power density by 51.51% compared to the initial condition. These findings demonstrate that high temperatures positively affect SOFCs' performance.

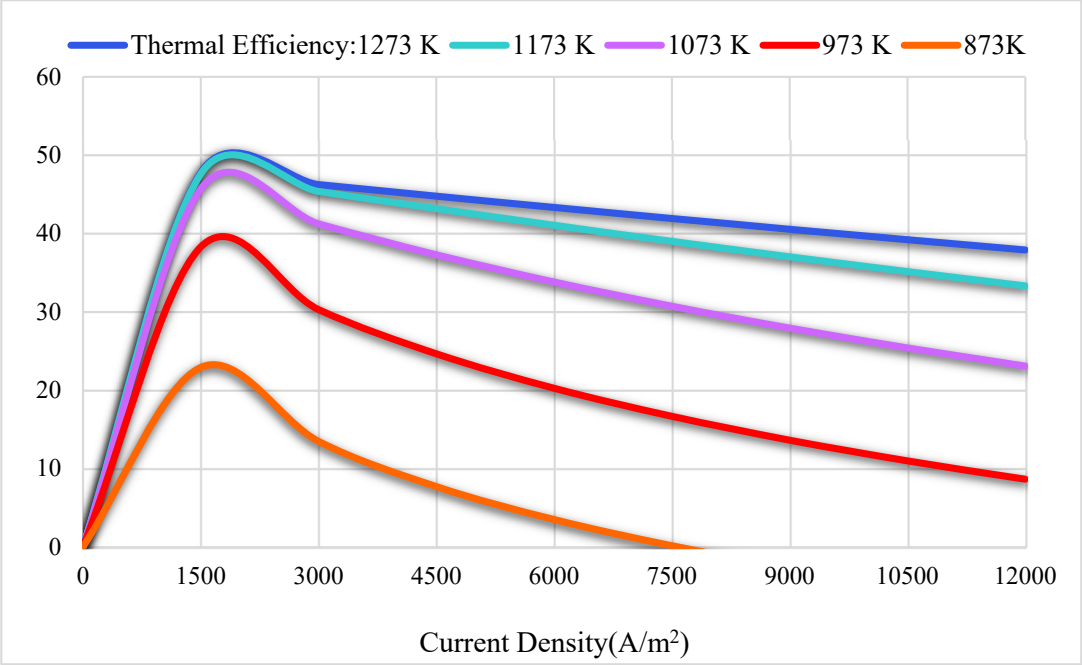

Figure 11. Thermal efficiency of SOFC at different temperatures.

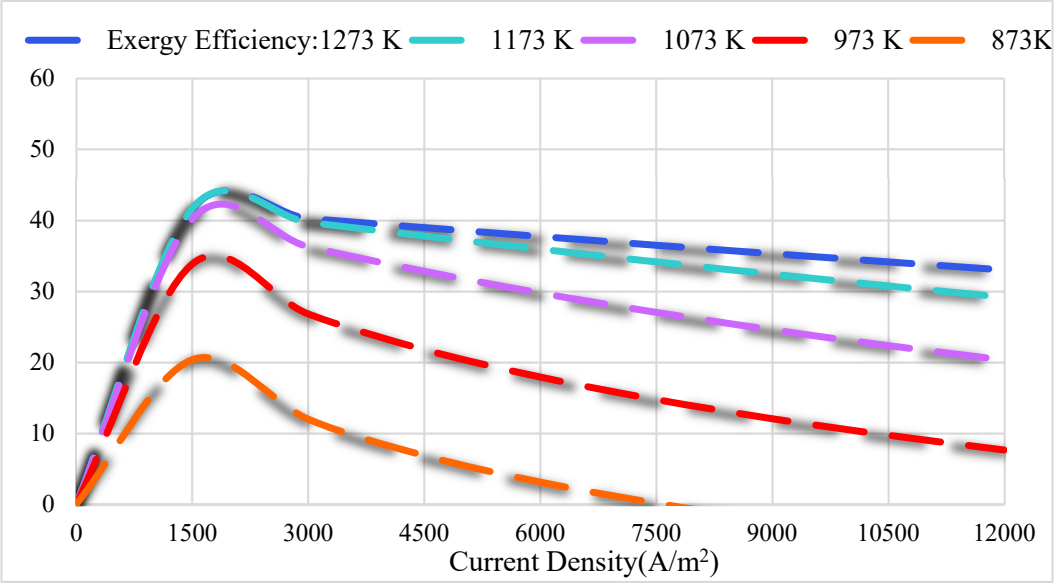

Figure 12. Exergy efficiency of SOFC at different temperatures.

4. Conclusions

In this study, a numerical model of a direct methane-fueled SOFC was developed, and both numerical and thermodynamic analyses were conducted. Energy and exergy calculations were made within the scope of thermodynamic analysis. It was observed that the increase in temperature increased the cell potential, and therefore, the power density increased. Under a constant current density, the voltage and power density values were 1.0081 V, 1.0543 V, 2337.13 W/m^2, and 2554.72 W/m^2 at operating temperatures of 1073 K and 1273 K, respectively. In addition, entropy production, which is an important parameter in exergy analysis, decreased with increasing temperature. At 3000 A/m^2 current density, the entropy production at an operating temperature of 873 K was 22 kW/K, while it was 15.30 kW/K at 1173 K. The results of the numerical and thermodynamic analyses were compared, showing highly consistent outcomes. Additionally, the effect of temperature on performance was examined through numerical results along with graphs depicting methane mole distribution and electrolyte current density. The numerical study revealed that an increase in temperature led to an increase in methane consumption rate due to the increased effects of factors such as reaction kinetics, diffusion, conductivity, and thermokinetic factors. Simultaneously, it was observed that this increase in temperature also resulted in a rapid increase in electrolyte current density. The study is expected to be very important in terms of examining the effect of temperature variation on exergy analysis in SOFC and verifying the numerical and theoretical results.

Author Contributions: Conceptualization, B.K., N.N.A., B.D., S.O., P.D. and I.B.; methodology, B.K., N.N.A., B.D., S.O., P.D. and I.B.; software, B.K., N.N.A., B.D., S.O., P.D. and I.B.; validation, B.K., N.N.A., B.D., S.O., P.D. and I.B.; investigation, B.K., N.N.A., B.D., S.O., P.D. and I.B.; resources, B.K., N.N.A., B.D., S.O., P.D. and I.B.; writing—original draft preparation, B.K., N.N.A., B.D., S.O., P.D. and I.B.; writing—review and editing, B.K., N.N.A., B.D., S.O., P.D., and I.B.; visualization, B.K., N.N.A., B.D., S.O., P.D. and I.B. All authors have read and agreed to the published version of the manuscript.

Funding: This research received no external funding.

Data Availability Statement: The raw data supporting the conclusions of this article will be made available by the authors on request.

Conflicts of Interest: The authors declare no conflicts of interest.

References

1. Vielstich, W.; Lamm, A.H.G. *Handbook of Fuel Cells: Fundamentals, Technology, Applications*; John Wiley & Sons, Ltd.: Hoboken, NJ, USA, 2003.
2. Halis, S.; Atak, N.N.; Doğan, B. Investigation of the performance of cathode supported solid oxide fuel cell with energy and exergy analysis at different operating temperatures. *Int. J. Energy Stud.* **2024**, *9*, 21–42. [CrossRef]
3. Altindal, S.; Erol, E.G.; Gurel, B. Numerical analysis of the effects of interconnector design and operating parameters on solid oxide fuel cell performance. *Int. J. Hydrogen Energy* **2024**, *52*, 1475–1490. [CrossRef]
4. Jiang, X.; Xu, Q.; Shi, Y.; Li, X.; Zhou, W.; Xu, H.; Zhang, Q. Synthesis and properties of Sm^{3+}-deficient $Sm_{1-x}BaCo_2O_{5+\delta}$ perovskite oxides as cathode materials. *Int. J. Hydrogen Energy* **2014**, *39*, 10817–10823. [CrossRef]
5. Yatoo, M.A.; Kawale, S.S.; Skinner, S.J. Perovskite and layered oxide materials for intermediate temperature solid oxide fuel cells. In *Intermediate Temperature Solid Oxide Fuel Cells*; Elsevier: Amsterdam, The Netherlands, 2020; pp. 315–346.
6. Xie, Y.; Ding, H.; Xue, X. Direct methane fueled solid oxide fuel cell model with detailed reforming reactions. *Chem. Eng. J.* **2013**, *228*, 917–924. [CrossRef]
7. Konwar, D.; Yoon, H.H. A methane-fueled SOFC based on a thin $BaZr_{0.1}Ce_{0.7}Y_{0.1}Yb_{0.1}O_{3-\delta}$ electrolyte film and a $LaNi_{0.6}Co_{0.4}O_3$ anode functional layer. *J. Mater. Chem. A* **2016**, *4*, 5102–5106. [CrossRef]
8. Mehrabian, M.; Mahmoudimehr, J. A numerical study to determine proper steam-to-fuel ratio in a biogas-fueled solid oxide fuel cell for different levels of biogas methane content. *Proc. Inst. Mech. Eng. Part C J. Mech. Eng. Sci.* **2023**, *238*, 2439–2455. [CrossRef]
9. Hu, F.; Chen, K.; Ling, Y.; Huang, Y.; Zhao, S.; Wang, S.; Gui, L.; He, B.; Zhao, L. Smart Dual-Exsolved Self-Assembled Anode Enables Efficient and Robust Methane-Fueled Solid Oxide Fuel Cells. *Adv. Sci.* **2024**, *11*, 2306845. [CrossRef]
10. Fragiacomo, P.; Piraino, F.; Genovese, M.; Corigliano, O.; De Lorenzo, G. Experimental Activities on a Hydrogen-Powered Solid Oxide Fuel Cell System and Guidelines for Its Implementation in Aviation and Maritime Sectors. *Energies* **2023**, *16*, 5671. [CrossRef]

11. Höber, M.; Königshofer, B.; Schröttner, H.; Fitzek, H.; Menzler, N.H.; Hochenauer, C.; Subotić, V. Experimental identification of the impact of direct internal and external methane reforming on SOFC by detailed online monitoring and supporting measurements. *J. Power Sources* **2023**, *581*, 233449. [CrossRef]
12. Zhang, P.; Yang, Z.; Jin, Y.; Liu, C.; Lei, Z.; Chen, F.; Peng, S. Progress report on the catalyst layers for hydrocarbon-fueled SOFCs. *Int. J. Hydrogen Energy* **2021**, *46*, 39369–39386. [CrossRef]
13. Gong, C.; Xu, Y.; Cai, S.; Chi, B.; Tu, Z. Comparative study on thermodynamic analysis of solid oxide fuel cells supplied with methanol or ammonia. *Int. J. Hydrogen Energy* **2024**, *50*, 1293–1301. [CrossRef]
14. Rath, M.K.; Kossenko, A.; Kalashnikov, A.; Zinigrad, M. Novel anode current collector for hydrocarbon fuel solid oxide fuel cells. *Electrochim Acta* **2020**, *331*, 135271. [CrossRef]
15. Randolph, K.L.; Dean, A.M. Hydrocarbon fuel effects in solid-oxide fuel cell operation: An experimental and modeling study of n-hexane pyrolysis. *Phys. Chem. Chem. Phys.* **2007**, *9*, 4245–4258. [CrossRef]
16. Lin, Y.; Zhan, Z.; Liu, J.; Barnett, S.A. Direct operation of solid oxide fuel cells with methane fuel. *Solid State Ion.* **2005**, *176*, 1827–1835. [CrossRef]
17. Dokamaingam, P.; Assabumrungrat, S.; Soottitantawat, A.; Sramala, I.; Laosiripojana, N. Modeling of SOFC with indirect internal reforming operation: Comparison of conventional packed-bed and catalytic coated-wall internal reformer. *Int. J. Hydrogen Energy* **2009**, *34*, 410–421. [CrossRef]
18. Fu, Q.; Li, Z.; Liu, Z.; Wei, W. Performance study of solid oxide fuel cell with Ni-foam indirect internal reformer: Intrinsic reforming kinetics and temperature uniformity. *Chem. Eng. J.* **2023**, *457*, 141170. [CrossRef]
19. Wójcik, M.; Szabłowski, Ł.; Dybiński, O. Comparison of mathematical models of steam methane reforming process for the needs of fuel cells. *Int. J. Hydrogen Energy* **2024**, *52*, 965–982. [CrossRef]
20. Aguiar, P.; Chadwick, D.; Kershenbaum, L. Modelling of an indirect internal reforming solid oxide fuel cell. *Chem. Eng. Sci.* **2002**, *57*, 1665–1677. [CrossRef]
21. Dokmaingam, P.; Assabumrungrat, S.; Soottitantawat, A.; Laosiripojana, N. Modelling of tubular-designed solid oxide fuel cell with indirect internal reforming operation fed by different primary fuels. *J. Power Sources* **2010**, *195*, 69–78. [CrossRef]
22. Klein, J.M.; Hénault, M.; Roux, C.; Bultel, Y.; Georges, S. Direct methane solid oxide fuel cell working by gradual internal steam reforming: Analysis of operation. *J. Power Sources* **2009**, *193*, 331–337. [CrossRef]
23. Murray, E.; Tsai, T.; Barnett, S.A. A direct-methane fuel cell with a ceria-based anode. *Nature* **1999**, *400*, 649–651. [CrossRef]
24. Saebea, D.; Authayanun, S.; Patcharavorachot, Y. Performance analysis of direct steam reforming of methane in SOFC with SDC-based electrolyte. *Energy Rep.* **2020**, *6*, 391–396. [CrossRef]
25. Tu, B.; Yin, Y.; Zhang, F.; Su, X.; Lyu, X.; Cheng, M. High performance of direct methane-fuelled solid oxide fuel cell with samarium modified nickel-based anode. *Int. J. Hydrogen Energy* **2020**, *45*, 27587–27596. [CrossRef]
26. Hu, Y.; Han, C.; Li, W.; Hu, Q.; Wu, H. Experimental evaluation of SOFC fuel adaptability and power generation performance based on MSR. *Fuel Process. Technol.* **2023**, *250*, 107919. [CrossRef]
27. Saadabadi, S.A.; Illathukandy, B.; Aravind, P.V. Direct internal methane reforming in biogas fuelled solid oxide fuel cell; the influence of operating parameters. *Energy Sci. Eng.* **2021**, *9*, 1232–1248. [CrossRef]
28. Sugihara, S.; Iwai, H. Experimental investigation of temperature distribution of planar solid oxide fuel cell: Effects of gas flow, power generation, and direct internal reforming. *Int. J. Hydrogen Energy* **2020**, *45*, 25227–25239. [CrossRef]
29. Lei, L.; Keels, J.M.; Tao, Z.; Zhang, J.; Chen, F. Thermodynamic and experimental assessment of proton conducting solid oxide fuel cells with internal methane steam reforming. *Appl. Energy* **2018**, *224*, 280–288. [CrossRef]
30. Wang, Z.; Fan, W.; Zhang, G. Comparison of the exergy efficiency of four power generation systems from methane using fuel cells. *RSC Adv.* **2017**, *7*, 39391–39402. [CrossRef]
31. Wang, Z.; Mao, J.; He, Z.; Liang, F. Energy-exergy analysis of an integrated small-scale LT-PEMFC based on steam methane reforming process. *Energy Convers. Manag.* **2021**, *246*, 114685. [CrossRef]
32. Heidarshenas, B.; Abdullah, M.M.; Sajadi, S.M.; Yuan, Y.; Malekshah, E.H.; Aybar, H. Exergy and environmental analysis of SOFC-based system including reformers and heat recovery approaches to establish hydrogen-rich streams with least exergy loss. *Int. J. Hydrogen Energy* **2024**, *52*, 845–853. [CrossRef]
33. Singh, U.R.; Bhogilla, S. Exergy analysis of reversible sofc coupled with organic Rankine cycle and hydrogen storage for renewable energy storage. *Int. J. Hydrogen Energy* **2023**, *48*, 39169–39181. [CrossRef]
34. Hussain, J.; Ali, R.; Akhtar, M.N.; Jaffery, M.H.; Shakir, I.; Raza, R. Modeling and simulation of planar SOFC to study the electrochemical properties. *Curr. Appl. Phys.* **2020**, *20*, 660–672. [CrossRef]
35. Xie, Y.; Ding, H.; Xue, X. Multi-physicochemical modeling of direct methane fueled solid oxide fuel cells. *J. Power Sources* **2013**, *241*, 718–727. [CrossRef]
36. Chaudhary, T.N.; Mehmood, M.; Saleem, U.; Abbasi, M.S.; Chen, B. Modeling of thermal impacts in a single direct methane steam reforming solid oxide fuel cell. *J. Power Sources* **2020**, *472*, 228605. [CrossRef]
37. Iliev, I.K.; Gizzatullin, A.R.; Filimonova, A.A.; Chichirova, N.D.; Beloev, I.H. Numerical Simulation of Processes in an Electrochemical Cell Using COMSOL Multiphysics. *Energies* **2023**, *16*, 7265. [CrossRef]
38. Zhao, F.; Virkar, A.V. Dependence of polarization in anode-supported solid oxide fuel cells on various cell parameters. *J. Power Sources* **2005**, *141*, 79–95. [CrossRef]

39. Wang, Z.; Lan, Q.; Zhang, D.; Li, M.; Cui, D.; Han, F. Optimizing ammonia-fueled planar SOFCs for low-temperature operation: Multiphysics simulation and performance sensitivity analysis. *Appl. Therm. Eng.* **2024**, *242*, 122442. [CrossRef]
40. Ni, M.; Leung, M.K.H.; Leung, D.Y.C. Parametric study of solid oxide fuel cell performance. *Energy Convers. Manag.* **2007**, *48*, 1525–1535. [CrossRef]
41. Chan, S.H.; Ho, H.K.; Tian, Y. Multi-level modeling of SOFC-gas turbine hybrid system. *Int. J. Hydrogen Energy* **2003**, *28*, 889–900. [CrossRef]
42. Chan, S.H.; Xia, Z.T. Polarization effects in electrolyte/electrode-supported solid oxide fuel cells. *J. Appl. Electrochem.* **2002**, *32*, 339–347. [CrossRef]
43. Ferguson, J.R.; Fiard, J.M.; Herbin, R. Three-dimensional numerical simulation for various geometries of solid oxide fuel cells. *J. Power Sources* **1996**, *58*, 109–122. [CrossRef]
44. Liu, Z.; Tao, T.; Deng, C.; Yang, S. Proposal and analysis of a novel CCHP system based on SOFC for coalbed methane recovery. *Energy* **2023**, *283*, 128996. [CrossRef]
45. Chan, S.H.; Khor, K.A.; Xia, Z.T. Complete polarization model of a solid oxide fuel cell and its sensitivity to the change of cell component thickness. *J. Power Sources* **2001**, *93*, 130–140. [CrossRef]
46. Akikur, R.K.; Saidur, R.; Ping, H.W.; Ullah, K.R. Performance analysis of a co-generation system using solar energy and SOFC technology. *Energy Convers. Manag.* **2014**, *79*, 415–430. [CrossRef]
47. Akkaya, A.V. Performance Analysis of Solid Oxide Fuel Cell Based Energy Generation Systems with Alternative Criteria. Ph.D. Thesis, Yıldız Teknik Üniversitesi, Esenler, Turkiye, 2007.
48. Sadeghi, M.; Jafari, M.; Hajimolana, Y.S.; Woudstra, T.; Aravind, P.V. Size and exergy assessment of solid oxide fuel cell-based H2-fed power generation system with alternative electrolytes: A comparative study. *Energy Convers. Manag.* **2021**, *228*, 113681. [CrossRef]
49. Sadeghi, M.; Nemati, A.; Ghavimi, A.; Yari, M. Thermodynamic analysis and multi-objective optimization of various ORC (organic Rankine cycle) configurations using zeotropic mixtures. *Energy* **2016**, *109*, 791–802. [CrossRef]
50. Ranjbar, F.; Chitsaz, A.; Mahmoudi, S.M.S.; Khalilarya, S.; Rosen, M.A. Energy and exergy assessments of a novel trigeneration system based on a solid oxide fuel cell. *Energy Convers. Manag.* **2014**, *87*, 318–327. [CrossRef]
51. Hanapi, S.; Tijani, A.S.; Rahim, A.H.A.; Mohamed, W.A.N.W. *Exergy Efficiency Profile of A 1kW Open Cathode Fuel Cell with Pressure and Temperature Variations*; Elsevier B.V.: Amsterdam, The Netherlands, 2015; Volume 79. [CrossRef]
52. Liu, J.; Barnett, S.A. Operation of anode-supported solid oxide fuel cells on methane and natural gas. *Solid State Ion.* **2003**, *158*, 11–16. [CrossRef]
53. Tu, B.; Wen, H.; Yin, Y.; Zhang, F.; Su, X.; Cui, D.; Cheng, M. Thermodynamic analysis and experimental study of electrode reactions and open circuit voltages for methane-fuelled SOFC. *Int. J. Hydrogen Energy* **2020**, *45*, 34069–34079. [CrossRef]